Radiation environment and doses on Mars at Oxia Planum and Mawrth Vallis: support for exploration at sites with high biosignature preservation potential

F. da Pieve, G. Gronoff, J. Guo, C. J. Mertens, L. Neary, B. Gu, N. E. Koval, J. Kohanoff, A. C. Vandaele, F. Cleri

JGR Planets

RESEARCH ARTICLE

10.1029/2020JE006488

Key Points:

- We study the radiation environment induced by galactic and solar radiation at Oxia Planum and Mawrth Vallis, for solar maximum/minimum
- Doses for solar maximum/minimum and their variation on surface pressure are compared to an updated analysis of Radiation Assessment Detector (RAD) data and previous results
- Slightly different water amounts in the regolith affect backscattered gamma-rays; exposure for long/short stays implies moderate/low risk

Correspondence to:

F. Da Pieve,
fabiana.dapieve@gmail.com

Citation:

Da Pieve, F., Gronoff, G., Guo, J., Mertens, C. J., Neary, L., Gu, B., et al. (2021). Radiation environment and doses on Mars at Oxia Planum and Mawrth Vallis: Support for exploration at sites with high biosignature preservation potential. *Journal of Geophysical Research: Planets*, *126*, e2020JE006488. https://doi.org/10.1029/2020JE006488

Received 1 MAY 2020
Accepted 17 NOV 2020

Radiation Environment and Doses on Mars at Oxia Planum and Mawrth Vallis: Support for Exploration at Sites With High Biosignature Preservation Potential

F. Da Pieve[1], G. Gronoff[2,3], J. Guo[4,5], C. J. Mertens[2], L. Neary[1], B. Gu[6], N. E. Koval[7], J. Kohanoff[6], A. C. Vandaele[1], and F. Cleri[8]

[1]Royal Belgian Institute for Space Aeronomy, BIRA-IASB, Brussels, Belgium, [2]NASA Langley Research Centre, Hampton, VA, USA, [3]Science Systems and Application Inc., Hampton, VA, USA, [4]School of Earth and Space Sciences, University of Science and Technology of China, Hefei, China, [5]CAS Center for Excellence in Comparative Planetology, USTC, Hefei, China, [6]Atomistic Simulation Centre, Queen's University Belfast, Belfast, UK, [7]CIC nanoGUNE BRTA, Donostia-San Sebastián, Spain, [8]Institute of Electronics, Microelectronics and Nanotechnology (IEMN, UMR 8520), Villeneuve d'Ascq, France

Abstract The first human missions on Mars will likely involve several astrobiology-driven science operations, at sites with high biosignature preservation potential. Here, we present a study of the radiation environment induced by Galactic Cosmic Rays and Solar Energetic Particles at Oxia Planum, landing site of the European Space Agency ExoMars 2022 mission, and at two different locations in Mawrth Vallis, using the Monte Carlo GEometry ANd Tracking 4-based code dMEREM (detailed Martian Energetic Radiation Environment Model). The radiation environment for solar minimum in 2009 and a period close to solar maximum during the declining phase of solar cycle 23 appears similar at the different sites, with the deepest Mawrth Vallis location having a slightly enhanced γ-ray contribution, due to a higher modulation of fast neutrons by the more water-rich regolith. The comparison with the Dose Equivalent from an updated extrapolation of 7+ years data from the Radiation Assessment Detector (RAD) onboard the Curiosity rover highlights the importance of input modulation conditions, some drawbacks of the galactic cosmic ray model used here, and the need to include heavy ions, the three aspects affecting differently the estimations for solar maximum and minimum. The dependence of doses on surface pressure highlights a possible influence of the different dust loading at the different sites. Estimated exposure levels for a 1-year stay and for a short stay in Arabia Terra, the latter including a October 28, 2003 event with a fluence an order of magnitude higher than the relevant September 2017 event detected by RAD, leave reasonable to large safety margins.

Plain Language Summary Space radiation is caused by high-energy particles coming from the Sun or further away. Such radiation is dangerous for humans since they can cause cancers. At Earth, we are protected by a relatively thick atmosphere and by the global magnetic field, but the first explorers of Mars will be subject to higher radiation exposure. In this paper, we compute the risks caused by these radiations at Oxia Planum, the landing site of the ExoMars 2022 mission, and Mawrth Vallis, previously under scrutiny by NASA and European Space Agency, both in the northern hemisphere. We modeled different conditions of space radiation (which is determined by the activity of the Sun) and we considered the effect of the ground composition on the results. The model results are compared with the estimations of the radiation at the ground based on the observations by the Curiosity rover located at the Gale crater in the Southern hemisphere. We show that locations rich in water may have more gamma rays. We show that the risks are moderate when considering the radiation exposure limits recommended for Low Earth Orbit.

1. Introduction

The first human missions to Mars will likely be astrobiology-driven, with explorers involved in contextual surveys, search of candidate mineralogical samples, and supervised drilling operations. Assessing the radiation environment and doses at sites with high biosignature preservation potential is thus of fundamental importance for both estimating the health risks of future human explorers and providing reference doses for the degradation/survival rates of biological molecules in search-for-life studies.

Oxia Planum and Mawrth Vallis, two regions near the northern boundary of Arabia Terra, offer excellent conditions for the search of biosignatures. Oxia Planum is the final selected landing site for the next European Space Agency (ESA) mission ExoMars 2020 (now ExoMars 2022), partially because of more suitable conditions for the technical constraints such as landing and traversability, and different specific locations in Mawrth Vallis have been previously considered as candidate landing sites for ExoMars 2022 (Bridges et al., 2017), the current Mars Science Laboratory (MSL; Rogers & Bandfield, 2009) and Mars 2020 mission (Gross et al., 2017). Based on near-infrared OMEGA (Observatoire pour la Minéralogie, l'Eau, les Glaces et l'Activité) data as well as CRISM (Compact Reconnaissance Imaging Spectrometer for Mars) data, the regional compositional mapping has revealed wide deposits of clays at both sites, in particular Mg/Fe phyllosilicates (Carter et al., 2013). In particular, Oxia Planum exhibits a layered, meters-thick nearly homogeneous Fe-Mg phyllosilicates deposit and some hematite, while Mawrth Vallis mostly displays Fe-smectites with multiple oxidation states and a relevant presence of several other hydrated minerals (Poulet et al., 2020), in principle making the site rewarding in terms of both scientific outcomes and In-Situ Resource Utilization (ISRU). Clays are known to play a major role in the association of organic matter with mineral matrices and in the stabilization and preservation of biological molecules (Keil & Mayer, 2014). About hematite, some studies have reported it has a beneficial role for the preservation of microscopic signatures of life (Allen et al., 2004), while others have reported that it offers low preservation of amino acids (dos Santos et al., 2016) and induces oxidation of organics (Ertem et al., 2017).

The radiation environment at the surface of Mars is constituted by primary Galactic Cosmic Rays (GCRs), the low intensity background radiation flux modulated by the 11-year solar cycle, and by sporadic, high fluxes of Solar Energetic Particles (SEPs), as well as by secondary particles produced in the atmosphere and the regolith via ionization, spallation and fragmentation processes. The high-energy GCRs can penetrate the standard spacecraft hulls, as well as potential planetary habitats and astronauts suits, producing dangerous secondary radiation particles, effective at either directly breaking DNA strands, or producing chemically active radicals in tissues that can also induce bond breaking. Late stochastic effects from non-lethal doses, such as cataracts, cancer, damages to the central nervous and/or cardiovascular system (Cucinotta et al., 2012a, 2012b) are observed over time as an increased likelihood of occurrence relative to the general population. SEPs are produced by transient events on the Sun, such as flares and/or Coronal Mass Ejections (CMEs), which trigger the acceleration of intense fluxes of (mostly) protons and electrons with energies below a few hundreds MeV. The relatively rapid rise in particles fluxes during such events and the possible occurrence of such events at any time in the solar cycle (Feynman et al., 1993, 2002) have implications for planning expeditions in which the explorers would drive considerable distances from their habitat. Events can last for hours up to many days, and give rise to deterministic effects, as the Acute Radiation Syndrome (Anno et al., 1989), skin injury, the depletion of blood-forming organs (BFOs), and death (Cucinotta et al., 2015; Wu et al., 2009).

There is now a relevant number of detailed studies on the radiation environment and doses induced by GCRs (De Angelis et al., 2006; Ehresmann et al., 2011; Gronoff et al., 2015; Guo et al., 2015; D. Hassler et al., 2012, 2014; Matthiä et al., 2016; McKenna-Lawlor, Gonçalves, Keating, Morgado, et al., 2012; Saganti et al., 2004; Schwadron, et al., 2010; L. Simonsen et al., 1990; L. C. Simonsen & Nealy, 1993) and SEPs on Mars (De Angelis et al., 2006; Guo, Zeitlin, et al., 2018; Guo, Wimmer-Schweingruber, et al., 2019; Jiggens et al., 2014; Kozarev et al., 2010; Norman et al., 2014; Townsend et al., 2011; L. C. Simonsen & Nealy, 1993; Zeitlin et al., 2018). Inter-comparisons between different radiation transport tools and detailed comparison to RAD measurements have been provided in several recent studies (Guo, Saša, et al., 2019a; Matthiä et al., 2016; Matthiä et al., 2017), the latter also summarizing the work performed by several teams (de Wet & Townsend, 2017; Flores-McLaughlin, 2017; Matthiä & Berger, 2017; Ratliff et al., 2017; Slaba & Stoffle, 2017). The majority of these studies is either focused on Gale crater, in the southern hemisphere, where Curiosity is operating with the MSL-RAD detector (D. Hassler et al., 2012, 2014; Grotzinger et al., 2012), or on average global or altitude-dependent radiation maps. A thorough analysis of the radiation environment at sites in the northern hemisphere, such as those at the northern boundary of Arabia Terra, is still to be done.

In this work, we provide a first assessment of the radiation environment and doses at Oxia Planum and Mawrth Vallis as induced by GCRs in solar minimum (January 2009, northern fall) and close to solar maximum during the declining phase of solar cycle 23 (October 2003, dusty northern winter), and by SEPs

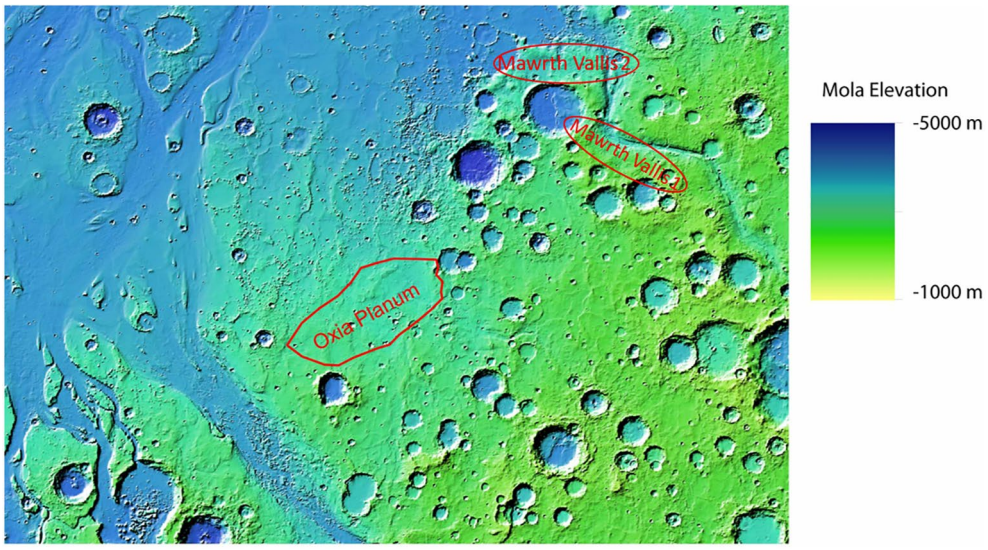

Figure 1. Topography MAP from Mars Global Surveyor, Mars Orbiter Laser Altimeter (MOLA). Copyright: NASA.

and background GCRs during the October 28, 2003 event. For Mawrth Vallis, the location previously under scrutiny by ESA, west to the main channel, denoted here Mawrth Vallis 1, and the location previously considered by NASA, in the north of Oyama crater, denoted Mawrth Vallis 2, are considered. The three sites have respectively elevation ∼−2600, ∼−2011 and ∼−3780 m and are depicted in the Mars Orbiter Laser Altimeter (MOLA) map in Figure 1. The radiation environment and different types of doses are obtained via the Monte Carlo GEometry ANd Tracking (Geant4)/PLANETOCOSMICS (Desorgher, 2005) ESA's tool dMEREM (Gonçalves et al., 2010; McKenna-Lawlor, Gonçalves, Keating, Morgado, et al., 2012; McKenna-Lawlor, Gonçalves, Keating, Reitz, et al., 2012). The results are compared with an updated extrapolation based on 7+ years of RAD data. The contribution of downward and backscattered radiation, the contribution of different particle type, and the variation of daily dose rates with surface pressure during the two solar modulation periods are investigated. We focus in particular on the absorbed dose, the main dosimetric quantity related directly to energy deposition in a target (locally), the Ambient Dose Equivalent (ADE), an operational quantity for measurements and radiation protection, and on the Effective Dose (ED), which is the relevant quantity for stochastic effects. Results for long and short stays, the latter including the occurrence of the October 28, 2003 SEP event, are compared to the radiation exposure limits usually recommended and to the relevant September 2017 event detected by RAD.

Table 1
Average Percentage by Weight of the Constituents Present as Derived From GRS Data at the Three Specific Sites Considered in This Work

Mineral	Oxia Planum −2600.00 m	Mawrth Vallis site 1 −2011.00 m	Mawrth Vallis site 2 −3875.00 m
SiO_2	47.23	47.44	47.37
Fe_2O_3	16.72	16.49	16.05
Bulk Al_2O_3, MgO, CaO, Na_2O, K_2O	32.10	32.10	32.10
H_2O	3.95	3.97	4.48
Density (g/cm^2)	1.80	1.82	1.80

2. Model Description

2.1. dMEREM, Regolith Composition and Atmospheric Parameters

dMEREM, also implemented in the ESA's Space Environment Information System (SPENVIS) (Heynderickx et al., 2004; Kruglanski et al., 2009), was used in standalone mode to perform the Monte Carlo calculations of the transport of GCRs (protons+α-particles) and SEPs (protons) through the atmosphere and regolith. dMEREM incorporates PLANETOCOSMICS (Desorgher, 2005), based on GEANT4 (Agostinelli et al., 2003).

The regolith composition of the three sites considered in this work is based on data from the Gamma Ray Spectrometer (GRS) aboard Mars Odyssey and it is reported in Table 1. Some small differences in the regolith composition can be noticed, with Oxia Planum having more Fe_2O_3 (hematite), and Mawrth Vallis site 2 having less hematite but more wa-

ter. The variation are ∼10% in water-content and ∼4% in Fe-content. Topographic data are taken from the MOLA instrument onboard the Mars Global Surveyor (MGS) (Smith et al., 2001). The regolith is modeled as a 100 m deep layer and its composition is rather different from the one used in other studies for Gale Crater (Matthiä et al., 2016), that purely considers a default basaltic composition (SiO_2 51.2%, Fe_2O_3 9.3%, H_2O 7.4%), resembling a general terrestrial basalt (Nockolds, 1954).

Atmospheric temperature, density and composition were extracted at the three sites from the Mars Climate Database (MCD) (Forget et al., 1999, 2006), up to an atmospheric height being $h = 150$ km, using the default solar minimum scenario for January 2009, and the dusty solar maximum scenario and the baseline MY26 scenario for October 2003. A postprocessing software was used to combine the surface pressure data with MGS MOLA topography (Smith et al., 2001). The period of October 2003 (close to solar maximum) and January 2009 (solar minimum) correspond to northern winter and fall, respectively. Simulations are performed for local 2 a.m. and 2 p.m.

The QGSP_BIC_HP physics list is used, which uses a quark gluon string model for hadrons at high energies (>10 GeV), the binary intranuclear cascade model for nucleons at energies <10 GeV, and, for neutrons with energy <20 MeV, the G4NeutronHP model (based on the Evaluated Nuclear Data File- database). The low electromagnetic list (Livermore models) is used. The number of simulated primary particles was 10^6 per bin.

2.2. Radiological Quantities

In this work, we focus on the absorbed dose, the ADE and ED. The absorbed dose corresponds to the average energy deposited by energetic particles in a target (locally, e.g., at the point of interest) (Mertens, 2016). In biological targets, this is considered to be predominantly due to ionization energy loss:

$$D = \frac{\Delta E}{m} = \frac{1}{\rho}\int_{E_0}^{\infty} \frac{d\epsilon}{dx} f\left(E\right) dE \tag{1}$$

where m is the mass of the volume of interest in the target, $d\epsilon/dx$ is the (unrestricted) collisional stopping power (corresponding to the electronic stopping power, e.g., the energy lost by the particle per unit path length), $f(E)$ is the particle fluence (E being the energy of impacting particles), and ρ is the density in the volume of interest, for instance, a detector or a human organ. The unit of D is the Gray (where 1 Gy = 1 J kg^{-1}). In order to estimate the absorbed dose, not automatically printed by dMEREM, a water layer of a thickness of 10 cm was added at the ground and the energy deposition in that layer is scored, similarly to previous works (Gronoff et al., 2015).

The ED is the dose received by the full body and is expressed as the sum of the equivalent doses in all tissues and organs of the body, weighted by an organ/tissue weighting factor such that:

$$ED = \sum_T w_T H_T \tag{2}$$

where w_T is the weighting factor of tissue T and H_T is the equivalent dose for that tissue $H_T = \sum_R w_R D_{T,R}$, where $D_{T,R}$ is the average absorbed dose from radiation R in tissue or organ T, and w_R is the radiation weighting factor of radiation R, which varies according to particle type and energy (ICRP, 2010). The ED is measured in Sieverts (Sv).

In dMEREM, the alternate operational quantity ADE used in instrumental measurements is also implemented, as it avoids the complexities associated with phantoms or patient anatomy (Fontenot et al., 2009). The reference phantom is the International Commission on Radiation Units and Measurements (ICRU) sphere, a 30 cm-diameter sphere made of tissue equivalent material (density: 1 g/cm^3; mass composition of 76.2% O; 11.1% C; 10.1% H and 2.6% N). The ADE at a location of interest in a radiation field is defined as the Dose Equivalent (DE) which would be generated in an oriented and expanded radiation field at a depth of 1 cm on the radius of an ICRU Sphere, oriented so as to be opposite to the direction of the incident radiation (Casimiro et al., 2018; Osamu et al., 1999). Differently from the equivalent dose (not studied in this work), the DE is defined as a product of Q and D at a point in tissue, where D is the absorbed dose and Q the quality

factor at the point of interest, a function of unrestricted linear energy transfer (unrestricted LET, denoted as L below) in water.

Practically, in dMEREM the ADE is calculated by multiplying the fluences for each particle by previously calculated fluence-to-ambient dose equivalent conversion factors (tabulated in [Pelliccioni, 2000] and obtained with the FLUktuierende KAskade or Fluctuating Cascade) and adding all the contributions from the different particles i:

$$H_{10}^{(*)} = \sum_i H_i = \sum_i \sum_E f^i_{H^*(E)} \Phi_i(E) \tag{3}$$

The ED is also calculated in a similar manner, by applying previously calculated fluence-to-Effective Dose conversion factors applied to the distribution of particle fluence as a function of energy (Pelliccioni, 2000).

It is important to underline that the ADE and the DE reported in studies on RAD data are two distinct quantities. The latter is defined as $H_T(L) = Q_T(L) D_T(L)$, where $D_T(L)$ is the absorbed dose integrated in the volume of the organ or tissue T, and $Q(L)$ is the quality factor, while the ADE is calculated at a specific point in the tissue-equivalent phantom (the ICRU sphere).

2.3. Space Radiation Environment

The GCRs fluxes for protons and α-particles for solar minimum (January 2009) and close to solar maximum during the declining phase of solar cycle 23 (October 2003), obtained with the ISO-15390 model (Nymmik et al., 1996), are reported in Figure 2 (top panel). The spectra were retrieved from SPENVIS (Heynderickx et al., 2004; Kruglanski et al., 2009) and are considered as isotropic. Strong solar modulation as in October 2003 reduces the contribution of the low energy portion of GCRs protons and α-particles. Heavier primary ions have been ignored, since they contribute to only about 1% of the GCRs flux (Simpson, 1983) (and even less of the SEPs flux). However, it should be underlined that high-Z particles may interact with the atmosphere and generate secondaries, which would still contribute to the surface radiation exposure (Dartnell et al., 2007; Matthiä et al., 2016; Röstel et al., 2020).

The 28 October event and the series of events that took place at the end of October 2003-beginning of November 2003 were previously studied by several authors (Chenglong et al., 2008; Crider et al., 2005; Jiggens et al., 2014; Kozarev et al., 2010; Mewaldt et al., 2005). The differential proton fluxes for the October-November 2003 SEP events from the Geostationary Operational Environmental Satellite GOES-11 and retrieved from the Solar Energetic Particle Environment Modelling (SEPEM) reference event list (Jiggens et al., 2012) are reported in Figure 2 (middle panel). The largest solar proton enhancement occurred on the 28 October following an X17.2 class flare (Jiggens et al., 2014). This was the largest SEP event of the past 20 years in the tenths of MeV energy range (Jiggens et al., 2014). In principle, low energy SEP events are relatively shielded by the Martian atmosphere. Nevertheless, the October 28, 2003 event, which occurred during the northern dusty winter and which caused the unrecoverable failure of the Martian Radiation Environment Experiment (MARIE) instrument on board Mars Odyssey, is an interesting case to consider and to compare with the recent results reported for the September 2017 event, the most relevant event observed by MSL-RAD on Mars up to now (Guo, Dumbovi, et al., 2018a; D. M. Hassler et al., 2018; Zeitlin et al., 2018).

The magnetic connection between Earth and Mars was good for the series of SPEs during the end of October 2003-beginning November 2003. Here, near-Earth particle measurements from the GOES-11 spacecraft have been used as proxies to estimate the overall particle doses for the October 28, 2003 event, assuming the fluxes fell off as $1/r^2$ (where r is the helio-radial distance). In Figure 2 (bottom panel), points represent the fluences in each GOES channel, obtained by integrating the flux values for each channel over event duration and the fit has been obtained by double power-law function. Only protons have been considered for SEPs, being the dominant species in such events and thus posing the greatest short-term radiation damage risk. The event is considered to be isotropic upon arrival at Mars.

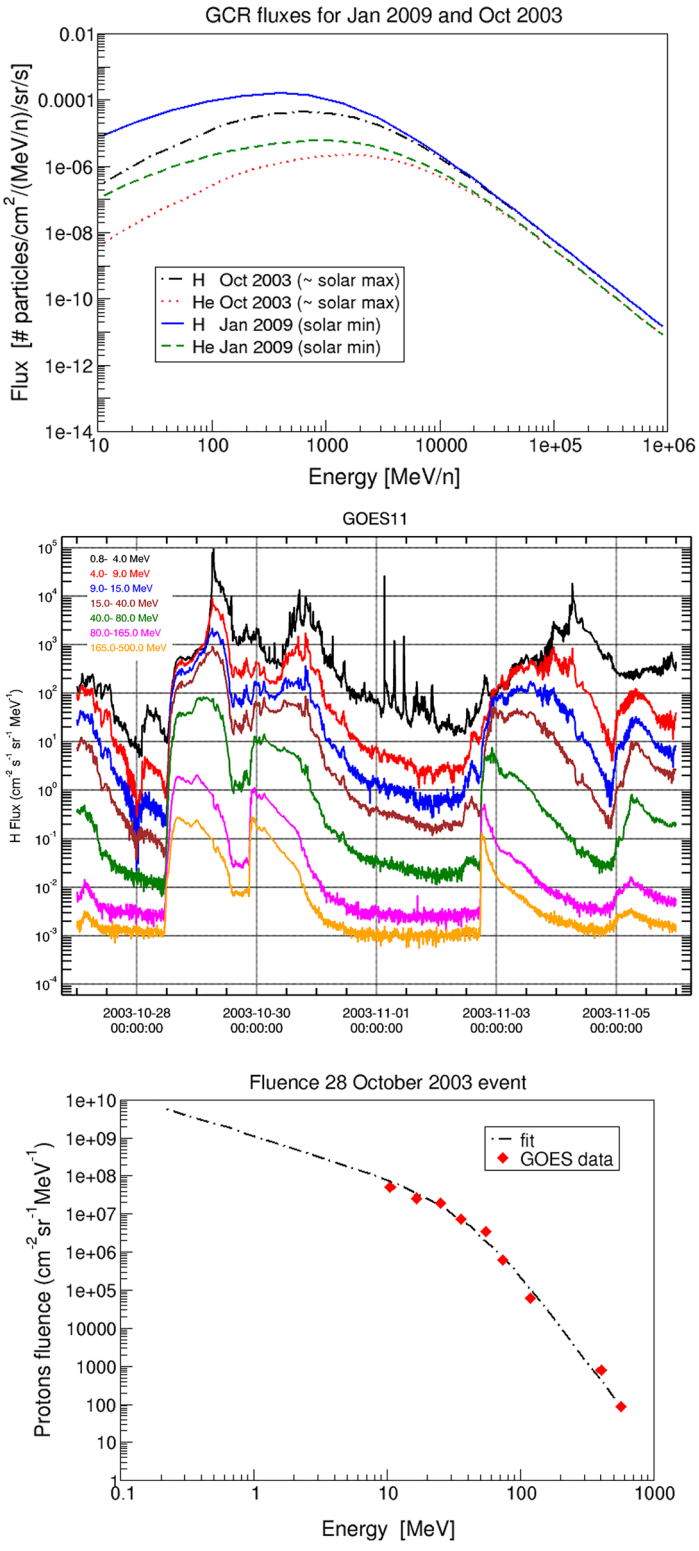

Figure 2. Top panel: Impacting GCRs protons and α-particles spectra during solar minimum in January 2009 and during early October 2003; middle panel: differential proton fluxes for the October–November 2003 SEP events, retrieved from the SEPEM reference event list (Jiggens et al., 2012); bottom panel: proton fluence spectra from GOES-11 for the October 28, 2003 event fitted with a double power-law function (spectral indexes 1.06, 4.26), following (Mewaldt et al., 2005). GCR, Galactic Cosmic Rays; GOES, Geostationary Operational Environmental Satellite; SEPEM, Solar Energetic Particle Environment Modelling.

Table 2
Comparison Between the ADE Rate (μ Sv/day) and the Absorbed Dose (μ Gy/day) From This Work (Averaged Over Day/Night and Induced by GCRs Protons + α -Particles During Solar Minimum and Close to Solar Maximum) With the DE and Absorbed Dose Obtained From an Updated Extrapolation of 7+ Years of RAD Data

			This work	Extrapol. RAD data	MARIE/Liulin-MO
dMEREM sol.min./~max. (January 2009/October 2003)					
Oxia Planum	ADE	(μSv/day)	632/356	-	-
Mawrth Vallis 1	ADE	(μSv/day)	634/360	-	-
Mawrth Vallis 2	ADE	(μSv/day)	611/348	-	-
Oxia Planum	abs.dose	(μGy/day)	230/110	-	-
Mawrth Vallis 1	abs.dose	(μGy/day)	250/122	-	-
Mawrth Vallis 2	abs.dose	(μGy/day)	193/100	-	-
extr.RAD data sol.min/~max.					
Gale crater	DE	(μSv/day)	-	745.9 ± 87.2/498.7 ± 76.3	-
Gale crater	abs.dose	(μGy/day)	-	310.8 ± 24.4/207.8 ± 24.1	-
MARIE data ~sol.max					
Orbit	abs.dose	(μGy/day)	-	-	*230.0*
Liulin-MO data 04/2016-03/2017					
Cruise	DE	(μSv/day)	-	-	*1970/2040 ± 400*
Orbit (MC01)	DE	(μSv/day)	-	-	*2230/2260.00 ± 500*
Orbit (MC02)	DE	(μSv/day)	-	-	*2300.00 ± 550*

Note. Values from the RAD analysis are given in plastics, no correction factor has been used as plastic is close to water in terms of its response to the energetic charged particles that dominate the radiation environment on Mars (Zeitlin et al., 2018). The DE from Liulin-MO measurements during ExoMars TGO cruise (Semkova et al., 2018) in 2016–2017 and the absorbed dose measured in September 2003 by the MARIE instrument on board Mars Odyssey are also reported (Zeitlin et al., 2010) (in *italics*, as data from Liulin-MO correspond to different solar modulation conditions with respect to those considered in the calculations, and data from MARIE are affected by the some materials of the spacecraft, see text). Uncertainty associated to dMEREM results is ~1%.

Abbreviation: ADE, Ambient Dose Equivalent; DE, Dose Equivalent; RAD, Radiation Assessment Detector; TGO, Trace Gas Orbiter.

3. Results

3.1. GCRs Induced Daily Dose Rates and Comparison With the Updated Extrapolation From 7+ Years of RAD Data

Table 2 presents a comparison between the ADE and absorbed dose daily rates (averaged over day/night) for GCRs and an updated extrapolation of the DE and absorbed dose rates based on 7+ years RAD data at Gale Crater, based on a similar previous analysis that was using fewer statistics (Guo et al., 2015). The comparison to the DE is only indicative, as here the ADE is calculated; nevertheless, we proceed as in previous works (McKenna-Lawlor, Gonçalves, Keating, Morgado, et al., 2012) where useful information was extracted by comparing the ADE with results on the DE from different works.

Our results for both solar minimum and close to solar maximum show very similar ADE average daily rates for Oxia Planum and Mawrth Vallis site 1, essentially coinciding within statistical uncertainty. The ADE average daily rate at Mawrth Vallis site 2, the location with the lowest elevation, is slightly lower with respect to the ADE rates at the other sites, in particular for solar minimum, due to a stronger shielding effect by the atmosphere. We note that our ADE average daily rates for the three sites are considerably lower than the updated analysis of 7+ years of RAD data for both solar maximum and solar minimum, but in fairly good agreement with the previous extrapolation based on fewer statistics for solar maximum (around ~350 μSv/day, not reported in Table 2) (Guo et al., 2015). The *absorbed* dose average daily rate obtained for a water slab of 10 cm at Oxia Planum is 230 μGy/day for solar minimum and 110 μGy/day close to solar maximum (early October 2003), with minimal variations at Mawrth Vallis 1 and slightly lower values at Mawrth Vallis

2 at lower elevation. We note an overall underestimation of the absorbed doses when compared with the extrapolated absorbed doses from the RAD analysis, similarly to the case of the comparison between the ADE and the DE.

The comparison of our results with those from the updated analysis of 7+ years of RAD data is affected by different factors, among which some differences between the initial modulation conditions given in input to our calculations and those on which the RAD analysis is based, the choice of a specific GCRs model and the neglect of heavier ions in our calculations. First, the GCRs model used by dMEREM (ISO 15390) uses as input the 12-month averages of sunspot numbers (SSNs), retrieved from the Solar Influences Data Analysis Center (SIDC) - Sunspot Index and Long-term Solar Observations (SILSO) (http://www.sidc.be/silso/, 99 for October 2003 and 4.8 for January 2009). The SSNs used for the RAD data analysis are the monthly mean SSNs, 97.8 and 1.3 for October 2003 and January 2009 respectively. Thus, the conditions under which the calculations here presented have been performed and those of the analysis of 7+ years of RAD data are almost equivalent for solar maximum, while for solar minimum the conditions are slightly different. An underestimation of doses for solar minimum could then be reasonably expected.

For what concerns the specific GCRs model, the ISO 15390 model used here has been reported to exhibit its own discrepancies with the measured flux for different near-Earth and space missions (Mrigakshi et al., 2012, 2013). In particular, for solar maximum periods, the ISO15390 model resulted in considerable overestimation of all investigated particle fluxes for different missions, for example, over 70% for hydrogen nuclei in comparison with the measurements of different missions and that it underestimates the flux at low energy. It may thus be expected that this would lead to an overestimation of dosimetric quantities induced by GCRs, which is actually not the case in our study. For the case of solar minimum, the ISO15390 model has been reported to derive lower GCR hydrogen fluxes, in comparison with the data measured by different near-Earth and space missions and in comparison to more accurate models such as the Badhwar-O'Neill 2010 model (Mrigakshi et al., 2012, 2013). Thus, for solar minimum, an additional underestimation of doses, due to intrinsic limitations of the input GCRs model, can be expected.

Last, it is important to underline that neglecting heavier ions implies that the associated downward cascade and eventual backscattered radiation are not considered. The influence of heavy ions on different dosimetric quantities has been analyzed in several recent works. Röstel et al. (2020) found that, on the surface of Mars, the heavy ion primary particles contribute 9% of absorbed dose rate in a thin silicon slab phantom, while this ratio is slightly lower in a water sphere phantom, ~8%. The heavy ion contribution to equivalent dose (not investigated here) was reported to be slightly larger, 11.5%. Other works (Mertens et al., 2016; Norman et al., 2016) investigated the influence of heavy-ion cosmic ray primaries at ~30 km altitude at Earth, which has similarities with the Martian surface, and reported that the contribution of heavy ions to the absorbed dose and DE at that altitude is ~20% and ~50% respectively, though some overestimation of the quality factor possibly due to an over prediction of the flux was affecting the results (Norman et al., 2016). For solar maximum, considering only protons and α-particles should be of minor concern, likely because of the reduced mean free path of heavier ions in the atmosphere, the latter having a higher depth at the perihelion season than during early northern autumn in solar minimum 2009. However, with increasing atmospheric depth there would be an increase in fragmentation processes in the downward cascade, generating neutrons which give a relevant contribution in particular to the ADE, thus making the neglect of ions likely a critical aspect for the ADE, even in solar maximum. For solar minimum, it is clear that several different effects affect our results, and the neglect of high energy heavy ions is a considerable approximation (especially for the site at the lowest elevation, where the downward cascade would be more relevant), while RAD measurements are obviously sensitive to all particles. Nevertheless, here below we continue considering only protons and α-particles, similarly to previous studies (Guo, Zeitlin, et al., 2018; Gronoff et al., 2015), and within such approximation we compare the results obtained at the different sites. As a last remark, as noted above, the definitions of the ADE and DE are different, and as also evident by the the discussion further in the text, also other works found ADE rates lower than the DE values for similar solar modulation conditions.

The absorbed dose recorded by the MARIE detector on board Mars Odyssey in September 2003, just before the unrecoverable failure of the instrument due to the 28 October event, and the DE recorded by the Liulin-MO detector during the cruise of the ExoMars Trace Gas Orbiter (TGO) spacecraft and recorded

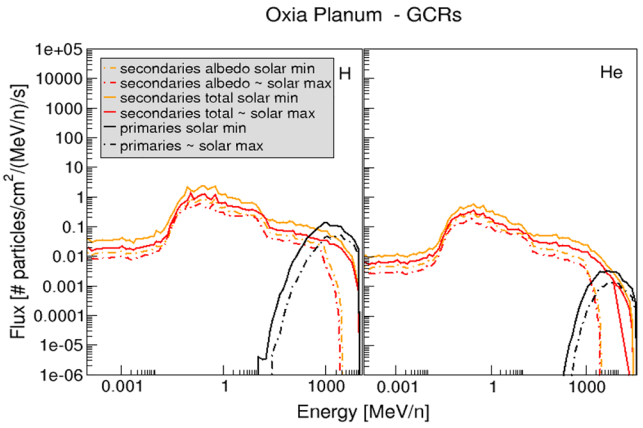

Figure 3. Primary and secondary (downward and albedo) radiation spectra at Oxia Planum induced by GCR protons and α-particles during solar minimum (solid lines) and close to solar maximum of solar cycle 23 (dash-dot lines).

by Liulin-MO in high elliptical orbit are reported in Table 2 only as an indicative reference. In principle, for October 2003, our surface absorbed dose appears to be slightly less than half of the absorbed doses recorded by MARIE, but both the planetary shielding effect, affecting the MARIE data as well as our results, and the fact that MARIE was covered by a 1.27 mm depth of aluminum and by a 100 μm depth of mylar thermal blanket (Zeitlin et al., 2010), thus not providing the fully unshielded dose in orbit, make it complicate to conclude on any impact of the sole atmospheric shielding effect on our results. The data from the TGO's cruise phase and the TGO orbits at high altitudes correspond to the declining phase of solar cycle 24. For high altitude orbits, the radiation conditions are very close to those in free space as shielding from Mars is negligible in such conditions. The difference between the cruise and orbit DE values can be interpreted mainly from the influence of the solar modulation (the cruise data are reported for April–September 2016, and the orbit data for November 2016–January 2017 and then February 2017–March 2017). Our ADE, for the declining phase of solar cycle 23, is ~1/6 of the DE by Liulin-MO in the declining phase of solar cycle 24, which is reasonable as the measurements by the latter correspond to periods with a weaker heliospheric activity with respect to October 2003.

3.2. Radiation Spectra and Contribution from Different Particle Type

The overall radiation spectra (in terms of primaries, secondaries, and secondaries albedo, and in terms of downward and upward particles) do not show clear appreciable different trends among the three sites, and thus only the spectra for Oxia Planum are reported, while the contribution from different particle type is reported for both Oxia Planum and the location at Mawrth Vallis which differs more from Oxia in terms of regolith composition, that is Mawrth Vallis 2.

The spectra of the primary and (total and backscattered) secondary particles, summed over all particles types, at Oxia Planum, induced by GCRs protons and α-particles, are reported in Figure 3, for solar minimum and close to solar maximum during the declining phase of solar cycle 23 (early October 2003, before the rise of the October–November 2003 events). For both protons and α-particles, there is a relevant contribution of the backscattered, albedo component, caused by the interaction of primary particles and downward secondaries with the martian regolith, to the secondary flux. Also, the spectrum of the secondaries (both downward and albedo) generated close to solar maximum closely follows the one for solar minimum, with variable differences around 100 MeV/n and a reduced overall intensity for solar maximum at lower energies. The spectra of the secondaries are very similar for primary impacting protons and α-particles. This is reasonable as a substantial amount of ^{4}He ions fragment into protons in the atmosphere and follow the same energy loss processes as for protons (Guo, Saša, et al., 2019a).

In Figure 4, we report the downward and backscattered radiation spectra at the surface, separated per particle type, at Oxia Planum. Higher fluxes of the downward protons and α-particles, slightly shifted to lower energies, occur for solar minimum, as for solar maximum the stronger solar modulation leads to a reduction of the lower energy portion of GCRs. The high energy part of the spectrum is dominated by downward protons and neutrons, while neutrons and γ-rays are the predominant particles at the surface for energies lower than 100 MeV/n. The γ-contribution strongly decreases below the electron contribution below few tenths of keV. By comparing Figures 3 and 4, it can be easily noticed that, in case of impacting protons, protons reaching the surface are mostly primary particles, with the exception of those with energies below ~10 MeV, which are likely generated in the interaction of the GCRs with the atmosphere.

In Figure 5, we plot the contribution of primaries, secondaries and particle type for Oxia Planum and Mawrth Vallis 2 to the ADE and ED hourly rate, for solar minimum and close to solar maximum, for impacting protons and α-particles separately. It can be observed that: (a) for the ADE, which is more sensitive to neutrons, primaries always contribute less than secondaries for both sites, and neutrons give the largest contribution for both sites and for both solar modulation periods; (b) for the ED, primaries contribute less than

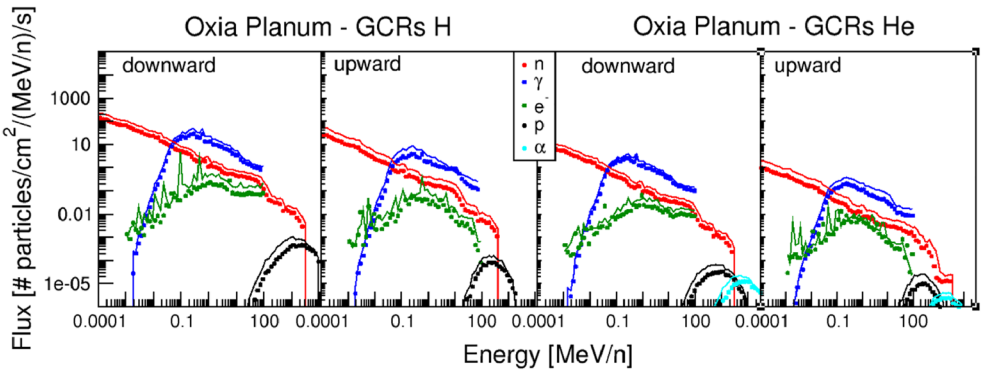

Figure 4. Radiation spectra at the surface of Mars at Oxia Planum as induced by GCR impacting protons and α-particles during solar minimum (January 2009) (solid lines) and close to solar maximum during the declining phase of solar cycle 23 (early October 2003) (circles): downward and upward contributions, separated for particle type. GCR, Galactic Cosmic Rays.

secondaries for both periods at Mawrth Vallis 2, suggesting the increased contribution of fragmentation secondary products to the ED; for Oxia Planum, primaries still contribute less than secondaries for solar maximum, but they contribute nearly to the same extent as secondaries for solar minimum; this suggests that at such higher elevation site more primary protons reach directly the surface, while for solar maximum the increased atmospheric depth likely still causes a considerable contribution from fragments. The ED is more sensitive to protons for proton impact and to neutrons for impact of α-particles, which is ascribed to the fact that α-particles have a smaller mean free path and are much more attenuated with depth; (c) there

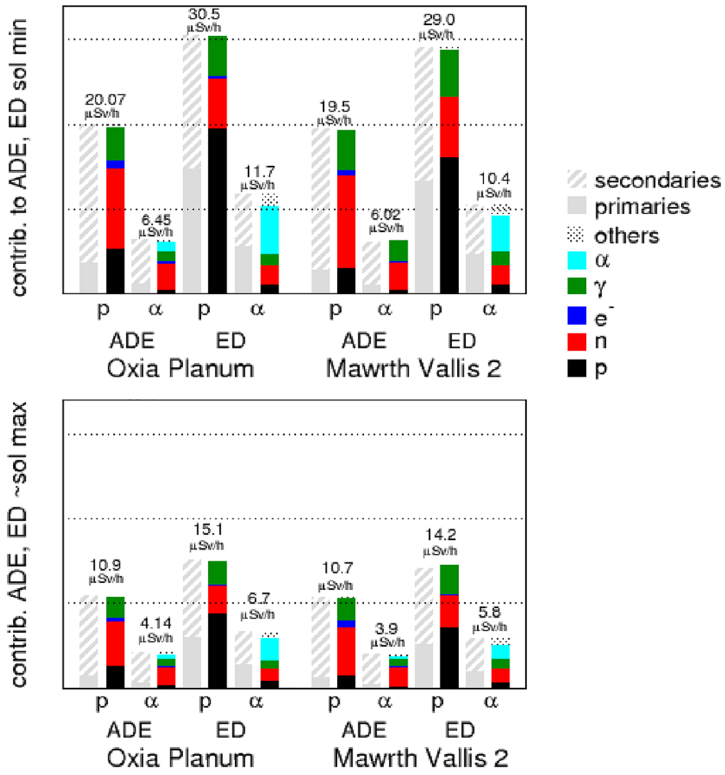

Figure 5. Contribution to ADE and ED hourly rate in terms of primaries and secondaries and in terms of particle type at Oxia Planum and Mawrth Vallis site 2, for solar minimum in January 2009 and close to solar maximum in October 2003. ADE, Ambient Dose Equivalent.

is a change in the contribution of γ-radiation, linked to the efficiency with which different amount water in the regolith moderate neutrons. Neutrons always contribute more at Mawrth Vallis 2 compared to Oxia Planum, because of the increase in downward fragmentation processes due to the increasing atmospheric depth. However, as water is a good neutron moderator (Röstel et al., 2020), the more hydrated soil at Mawrth Vallis 2 reduces the number of albedo neutrons, especially below about 10 MeV. This influences the amount and type of further secondaries particles generated by the interaction of such moderated neutrons with the other mineralogical components of the regolith. Most γ-rays originate from such reactions, as neutron inelastic scattering and thermal or epithermal neutron capture. In the upward flux, the strongest γ-rays lines are produced by non-elastic-scattering processes such as ^{56}Fe (n,nγ)^{56}Fe (0.85 MeV), ^{16}O (n,nγ)^{16}O (6.1 MeV), ^{28}Si(n,nγ)^{28}Si (strongest line at 1.8 MeV) and other higher energy γ-rays are produced by neutron capture processes such as ^{56}Fe (n,γ)^{57}Fe (7.6 MeV) and ^{28}Si(n,γ)^{29}Si (4.9 MeV). Looking at the γ-rays yield from the neutron capture ^{56}Fe (n,γ)^{57}Fe at the two sites, being Fe present in slightly different amount at the two sites, we notice an enhancement of such yield at Mawrth Vallis 2. This is indeed interpreted as due to the fact that more moderated neutrons are available for such neutron capture reaction, and is in line with earlier studies (Masarik & Reedy, 1996). The overall contribution of backscattered γ-rays to the ADE hourly rate at Oxia Planum changes from 20% to 22.4% between solar minimum and maximum, while it stays constant at 25% at Mawrth Vallis 2. The variation of γ-rays at sites of astrobiological interest is important as γ-rays remain the reference radiation for the estimation of degradation of biological molecules (Dartnell et al., 2007; Ertem et al., 2017; Pavlov et al., 2012, 2002). Also, this may be relevant in future considerations of valuable sites for exploration-related resources on Mars with a mineralogy dominated by hydrated minerals. Here, the difference in the backscattered γ-rays remains nevertheless small, as the smaller amount of downward neutrons at Oxia Planum, combined with a higher Fe-content, also helps in lowering the contribution of neutrons to ground doses (Keating & Gonçalves, 2012) and in giving rise to a similar γ-rays contribution. However, for the two sites considered here, the variation in Fe-content is only ~4%, and in water-content is ~10%, making water at Mawrth Vallis 2 a more efficient channel for neutrons modulation and following capture reactions by the Fe-oxide.

3.2.1. Dependence of GCR-Induced Doses on Diurnal Variations of Atmospheric Column Mass

Figure 6 (top panel) reports the day and night ADE and absorbed dose daily rates for Oxia Planum and Mawrth Vallis site 2, induced by GCRs protons and α-particles, for solar minimum and close to solar maximum, as a function of surface pressure. First, it can be noted that the pressure at each site is higher during the perihelion season (northern winter, October 2003) compared to the (early) autumn (January 2009), in agreement with the reports for different landing sites as a function of solar longitude (Martínez et al., 2017). The variation in the surface pressure however remains small at both sites, which is due to a non-optimal choice of the timing during day and night for which the calculations have been performed (2 a.m. and 2 p.m., not the peak-to-peak variation in the surface pressure daily cycle). Nevertheless, we observe that the day-night pressure variation for solar maximum is slightly higher compared to solar minimum, at least for Oxia Planum, as the solar forcing of tides increases when the amount of dust in the air rises (Leovy & Zurek, 1979; Medvedev et al., 2011). At Oxia Planum, the atmospheric column depth, directly linked to surface pressure from hydrostatic physics (Rafkin et al., 2014), varies from 20.37 g/cm^2 to 21.06 g/cm^2 for solar maximum, and from 18.08 to 18.56 g/cm^2 for solar minimum. Previous works have reported that, during northern winter, the increased dustiness of the atmosphere and the amplitudes of wave modes other than the sun-synchronous diurnal tide could tend to disrupt the diurnal tides propagation by modifying the atmospheric structure, reducing the pressure variation especially at low elevation sites with respect to higher elevation sites (Lee et al., 2009), which suggests that a smaller variation for Mawrth Vallis 2 could be expected.

A slightly higher surface pressure variation at Oxia Planum can also be expected looking at the vertical density profiles. These, as extracted from MCD (Figure 6, bottom panel), suggest that at Oxia Planum, for solar maximum, the density between 120 and 160 km (upper inset) and at the surface (bottom inset) differs more between day and night compared to what occurs at Mawrth Vallis 2. The visible optical depth, which reflects the variation in opacity due to dust loading in this case, also suggests that at Oxia Planum a higher dust opacity is present compared to Mawrth Vallis 2, with a higher variation between the chosen day and

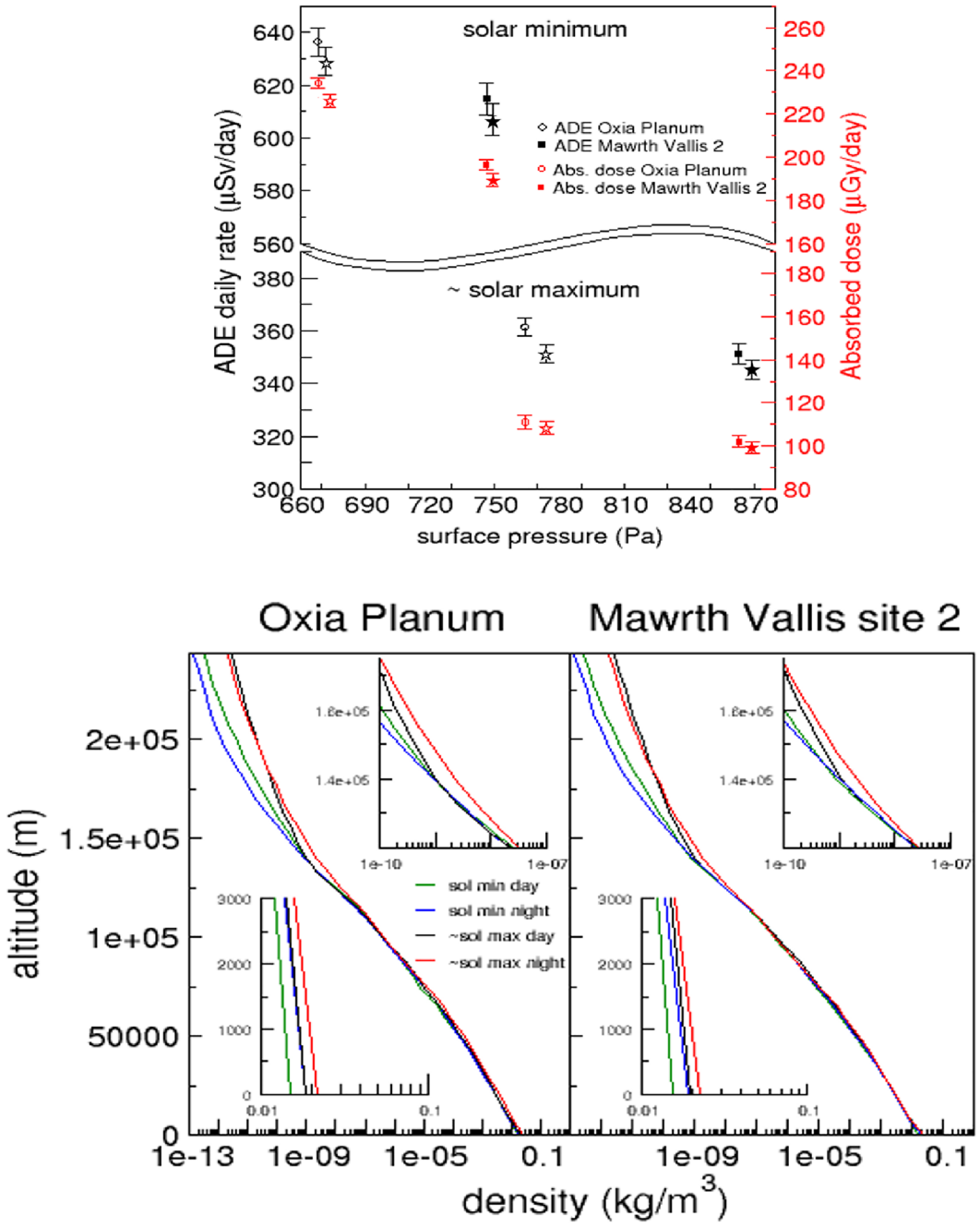

Figure 6. Top panel: ADE and absorbed dose day (circle or square) and night (star symbol) rates for the two sites as a function of day- and night-time surface pressure (statistical errors shown, known uncertainties associated with nuclear physics models used not considered); bottom panel: Vertical density profiles for different solar modulation periods above Oxia Planum and Mawrth Vallis site 2 (to be noted that in our calculations only a profile up to h = 150 km is considered). ADE, Ambient Dose Equivalent.

night time ($\tau = 1.54$ for vs. 1.60 for day and night respectively at Oxia Planum, and $\tau = 1.32$ and 1.34 for day and night respectively at Mawrth Vallis 2). Overall, looking at the sole extent of the variation of doses and of atmospheric depths, we observe that the (day/night averaged) atmospheric depth differs more between the two sites for solar maximum compared to solar minimum (by 3 g/cm^2 for solar maximum and 1.8 g/cm^2 for solar minimum); however, the ADE and the absorbed dose differ more, among the two sites, for solar minimum. This suggests that even a small difference in the averaged atmospheric column depth among the

two sites plays a relevant role in solar minimum, contributing in determining the efficiency of the shielding towards the low energy portion of the GCRs, unmodulated during solar minimum.

The results in Figure 6 (top panel) suggest an anti-correlation of the ADE and absorbed dose with surface pressure for both sites for solar minimum, in agreement with a previous analysis based on RAD data (Guo et al., 2017). Such anti-correlation can be well expected as, for lower surface pressure, despite the fewer neutrons generated in the downward cascade with such thinner atmosphere, more primary impacting ions can survive traversal, resulting in a measured higher dose rate. As the total column depth increases, the Martian atmosphere, despite being very thin, acts as a shielding layer against the incoming GCR flux, in particular the low energy portion of the flux which is more easily shielded by the atmosphere and which is more abundant in solar minimum. For the absorbed dose, we find a variation of 8 μGy/day out of a daily absorbed rate of ∼230 μGy/day for Oxia Planum, and of 6 μGy/day out of a daily absorbed rate of ∼193 μGy/day for Mawrth Vallis 2, in anti-correlation with surface pressure, similarly to the ADE. For the period close to solar maximum, we still find anti-correlation between the ADE day and night daily rate with surface pressure, which is in agreement with previous modeled results (Guo et al., 2017). The higher difference in the ADE day/night daily rate at Oxia Planum for solar maximum is due to the slightly higher difference in the density vertical profile compared to Mawrth Vallis 2. For the absorbed dose, we find an extremely weak anti-correlation of the absorbed dose rates with surface pressure for solar maximum, with a variation of only 2 μGy/day out of a daily absorbed rate of ∼110 μGy/day at Oxia Planum and a similar variation and absorbed dose for Mawrth Vallis 2. This is not in agreement with the correlation between absorbed dose and surface pressure expected on the basis of previous extrapolations for high solar modulation potentials (Guo et al., 2017), but the nearly coinciding absorbed dose rates suggest nevertheless a change in the dependence upon surface pressure.

Our lower estimation of the variations of the ADE and absorbed dose rates upon surface pressure with respect to RAD measurement is possibly also due to an amplification of the daily tide at Gale crater due to its peculiar topography. The variation of the absorbed dose rate measured by RAD over a diurnal cycle, which is ∼15 μGy/day peak to peak out of around 220 μGy/day for the period 2012–2014 (max Φ for this period 750 MV, with April 2014 maximum of solar cycle 24 [Guo et al., 2015]), corresponds to a daily pressure variation of ∼50 Pa as detected by the Rover Environmental Monitoring Station (REMS). Such variation is significantly larger than what observed at other landing sites on Mars and then what simulated for the Curiosity site by Global Circulation Models (GCMs) based on MCD - an averaged climate database. This is likely due to hydrostatic adjustment flows that amplify the daily tides and that are induced by the peculiar topography of the crater (Haberle et al., 2014; Richardson & Newman, 2018). However, when using actual GCMs with variability (Neary & Daerden, 2018) or mesoscale numerical models with sufficiently high horizontal resolution (grid spacing less than 5 km), then the large REMS daily pressure range are reproduced. Last, it should also be noted that the MCD atmospheric data used in this work inherently also have the seasonal CO_2 cycle, making impossible to distinguish the contribution to dose variation from the changes in atmospheric mass due to the CO_2 condensation cycle.

4. Scenarios for Short and Long Human Stays in Arabia Terra

The results in Table 3 consider two mission scenarios, one with a long stay on the surface of the planet (1-year) during solar minimum and close to solar maximum, and the other one being a short stay (30-days), during which we consider the October 28, 2003 event. We only report the results for Oxia Planum, as the results for the other sites do not change the conclusions with respect to the limits established for stochastic and deterministic effects. The estimations for a long stay at Oxia Planum provide support for the future measurements by the Liulin-ML detector on the ExoMars 2022 surface platform.

4.1. GCRs Contribution During a 1-Year Stay–Solar Minimum and Close to Solar Maximum

For a 1-year stay, scaling up to an entire year the contribution from GCRs, our results suggest that the ED for solar minimum, 368.4 mSv (see Table 3), is nearly the double of the ED close to solar maximum, 190.8 mSv. The ED limits for stochastic effects established by NASA (National Council on Radiation Protection and Measurements, Recommendations of Dose Limits for LEO, 2000) (620–1470 mSv for male and 470–1120

Table 3
Absorbed Dose (mGy), ADE/DE (mSv), and ED as Induced by GCRs (Protons and α) for a 1-Year, a 30-Day Stay During Quiet Times, and Short Stay Scenarios With an Occuring SEP Event

Mission	Absorbed Dose (mGy)	ADE, DE (mSv)	ED (mSv)
1-year GCR exposure			
Sol. min (or close to sol. min)			
dMEREM Oxia Planum (p+α)	84.0	230.4 (ADE)	368.4
Extrap. from RAD 7+ years	110 ± 4	265 ± 19	-
HZETRN L. Simonsen (1997) (p+α)	-	320.0	-
dMEREM M. Vallis McKenna-Lawlor, Gonçalves, Keating, Morgado, et al. (2012) (p+α)	-	186.9 (ADE)	518.8
Sol. max (or close to sol.max)			
dMEREM Oxia Planum (p+α)	38.7	131.8 (ADE)	190.8
Extrap. from RAD 7+ years	60 ± 4	144 ± 16	-
dMEREM M. Vallis McKenna-Lawlor, Gonçalves, Keating, Morgado, et al. (2012) (p+α)	-	103.0 (ADE)	278.0
Planetocosmics Gronoff et al 2015 (p+α)	40.15	-	-
HZETRN L. Simonsen 1997 (p+α)	-	150.00	-
30-days background GCR exposure sol max (or close to sol.max)			
dMEREM Oxia Planum (p+α)	3.0	10.8 (ADE)	15.7
dMEREM M. Vallis McKenna-Lawlor, Gonçalves, Keating, Morgado, et al. (2012) (p+α)	-	8.5 (ADE)	22.9
HZETRN Simonsen et al 1993 (p+α)	-	6.0-7.0/6.0-6.6 (skin/BFO)	-
GCR (p+α) + SEP (p)–short stay scenario			
dMEREM Oxia Planum (28 October 2003, 30 days, ~2.5-days SEP event)	8.4	22.2 (ADE)	30.6
dMEREM M. Vallis McKenna-Lawlor, Gonçalves, Keating, Morgado, et al. (2012) (April 2002, 30 days, 14-day SEP event)	-	8.8 (ADE)	23.1

Note. Values for GCRs are obtained by scaling up the average daily values. Comparison is with the updated extrapolation from 7+ years of RAD data, other results as computed using HZETRN (L. C. Simonsen & Nealy, 1993; L. Simonsen, 1997), PLANETOCOSMICS (Gronoff et al., 2015) and dMEREM (McKenna-Lawlor, Gonçalves, Keating, Morgado, et al., 2012). The results from (McKenna-Lawlor, Gonçalves, Keating, Morgado, et al., 2012) for a 30-day stay only in presence of GCRs have been extracted from Table 6 in (McKenna-Lawlor, Gonçalves, Keating, Morgado, et al., 2012) considering only protons and α-particles and for a period of 30 days assuming a constant distribution of GCRs flux. Uncertainty associated to dMEREM results is ~1%.
Abbreviations: ADE, Ambient Dose Equivalent; GCR, Galactic Cosmic Rays; HZETRN, High charge (Z) and Energy TRaNsport; SEP, Solar Energetic Particles.

mSv for a female, for increasing age at initial exposure) are not overpassed, for none of the two solar modulation periods. However, the ED is a considerable portion of the limit for young women. Considering that most of the exposure is during the trip to and back from Mars, additional shielding is obviously necessary to maintain dose levels at the Martian surface as low as possible (Röstel et al., 2020).

The obtained ADE in Table 3 (131.8 mSv/year and 230.4 mSv/year, respectively close to solar maximum and close to solar minimum) are close to the DE from the updated extrapolation from RAD data for the exact solar maximum and solar minimum, with a worsening of the agreement for solar minimum. The result for solar minimum is higher than a previous estimate by dMEREM for Mawrth Vallis (McKenna-Lawlor, Gonçalves, Keating, Morgado, et al., 2012), as it can be reasonably expected given the period considered in that work (2006, not exactly solar minimum) and the lower elevation of the specific location considered, but smaller than previous estimations in Simonsen, 1997 (L. Simonsen, 1997). However, a good agreement is obtained with the DE obtained for solar maximum from the same author (L. Simonsen, 1997). Several previous studies (Cucinotta et al., 2001; Ehresmann et al., 2011) reported higher values during solar minimum, in particular an annual GCRs-induced DE ranging from 200-300 mSv/year, depending on the altitude.

The yearly absorbed dose for a water slab of 10 cm at Oxia Planum is 84.0 and 38.7 mGy/year respectively for solar minimum and close to solar maximum (scaled up from the corresponding daily rates). As said above for the average daily rates, both these values are considerably smaller than the values obtained from

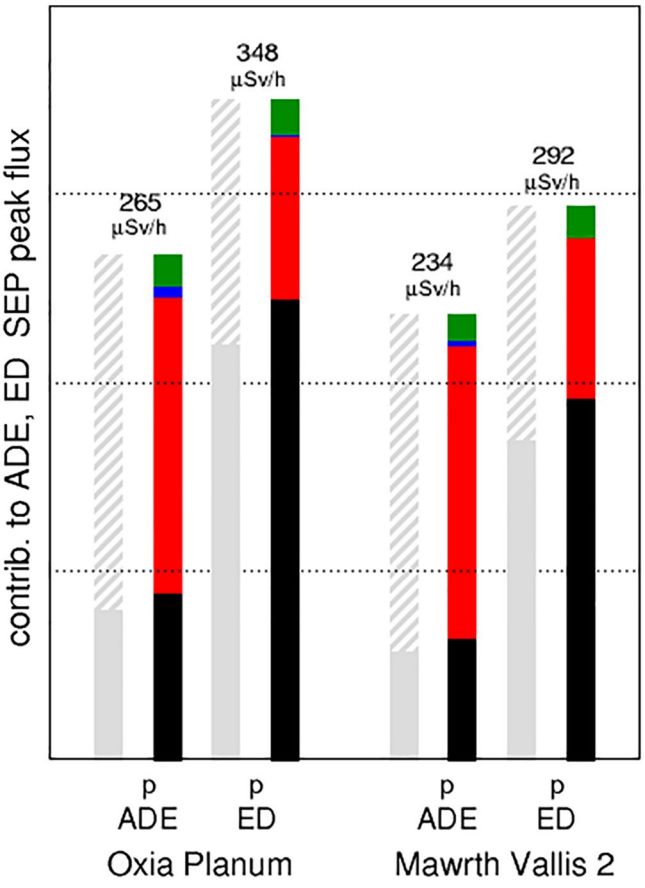

Figure 7. Contributions of the ADE and ED hourly rates for the peak flux of the October 28, 2003 SEP event. ADE, Ambient Dose Equivalent.

the updated extrapolation from 7+ years of RAD data, which is likely due to a mix of factors mentioned above (modulation conditions, choice of the GCR model, and neglect of the heavy ions). On the basis of previous studies (Norman et al., 2016; Röstel et al., 2020), however, the sole neglect of the heavier ions (and consequent generated downward cascade and backscattered radiation) would likely have a smaller impact on the absorbed dose results compared to the ADE.

4.2. GCRs and SEP Contribution During a 30-Day Stay Close to Solar Maximum

For a short 30-days stay during a period close to solar maximum, we find a GCRs-induced ADE which is higher than a previous estimate of the DE with the High charge (Z) and Energy TRaNsport (HZETRN) code (L. C. Simonsen & Nealy, 1993) for the solar maximum in 2014. This can be reasonably expected as in (L. C. Simonsen & Nealy, 1993) only atmospheric attenuation was taken into account but not the interaction of particles with the martian regolith, which leads to backscattering of neutrons and other secondary particles. Our ADE results are also higher than the results by dMEREM for solar maximum 2002 at Mawrth Vallis (a slightly different location in this region was considered) derived for a 30-day period from (McKenna-Lawlor, Gonçalves, Keating, Morgado, et al., 2012), likely because the period of October 2003, although close to maximum, is in the declining phase of the solar cycle 23.

The obtained peak absorbed dose rate for SEP protons from the October 28, 2003 event is 3.43 mGy/day. The influence of dust loading on the value of the peak absorbed rate can be estimated by comparing with the value obtained by using the baseline MY26 scenario, which has a visible optical depth for Oxia Planum $\tau = 0.78$ ($\tau = 0.67$ for Mawrth Vallis 2). The change in the absorbed dose at the ground is rather small, 6% at Oxia Planum. This variation is similar, although smaller, to the results from previous studies on different SEP events in different applicable dust loading conditions for sites in the southern hemisphere (Norman et al., 2014). In order to assess the risk for deterministic effects, the SEP protons-induced accumulated absorbed dose in a 10 g/cm^2 water target proxy for BFOs (obtained by multiplying the hourly averaged dose rate by 1 h and then summing all the doses for the full duration of the event [Chenglong et al., 2008], with a total of 5.06 mGy) has to be scaled by the Relative Biological Effectiveness (RBE) of protons (1.5 [Operational Radiation Safety Program for Astronauts in Low-Earth Orbit: A Basic Framework. Bethesda, Md., 2002]).

$$D(Gy - Eq) = D(Gy) \times RBE. \tag{4}$$

This yields exposures far below even the smallest of the 30-days exposure limits, which is 250 mGy-Eq for the heart and BFOs (Guidance on Radiation Received in Space Activities. Bethesda, Md., 1989; National Council on Radiation Protection and Measurements, Recommendations of Dose Limits for LEO, 2000). We can therefore infer that for the (sole) October 28, 2003 event the health risks to BFOs and the heart were minimal if explorers experienced these events with no/minimal shielding, despite its higher fluence compared to the relevant September 2017 event detected by RAD since landing (Zeitlin et al., 2018) (about one order of magnitude higher [Cohen & Mewaldt, 2018]).

Nevertheless, the series of events in October and November 2003 was very complex, with the onset of repetitive shocks lasting from October 19 through November 4, 2003 (Kozarev et al., 2010), with 10 shocks observed at the Advanced Composition Explorer (ACE) spacecraft and 5 CMEs (Lario et al., 2005). In a worst-case scenario of ~338 h of duration for the October-November 2003 events (http://spaceenv.esa.int/DataPlots/noaa/events/,June2007), there would have been also a considerable contribution to the ED to be

considered for late stochastic effects, to be added to the contribution induced by background GCRs. It is interesting to consider how the contributions of SEP primaries, secondaries and of particles type to the ADE and ED hourly rate during the SEP event, reported in Figure 7, change with respect to the GCRs-induced contributions in Figure 5. First, we notice that the ADE hourly rates are ∼22–24 times the ADE hourly rate induced by GCRs protons. The ADE hourly rates induced by the SEP peak flux differs more among the two sites compared to what occurs for background GCRs-induced ADE hourly rates, as the atmosphere modulates in a stronger way the lower energy SEPs flux, while the different amount of atmosphere to be traversed for the different sites is of lower importance for the transport of GCRs, especially for the (unmodulated) high energy portion. Close to solar maximum, primaries contribute less than secondaries to the ADE hourly rate, as it happens for background GCRs in early October 2003 (Figure 5), while for the ED, primaries contribute more than secondaries, for both sites, contrarily to the case of GCRs background radiation. This change too is interpreted as due to the fact that the low energy SEP proton flux is more strongly modulated by the atmosphere with respect to the background high energy portion of GCRs (unmodulated during solar maximum), and the protons generated in the fragmentation of such low energy SEP flux portion contribute to the ED more than secondaries. Last, similarly to the case of GCRs, we observe that a slighly higher contribution of overall neutrons is present at Mawrth Vallis 2, again induced by a more relevant generation of the downward cascade, and that also the relative contribution of γ-rays remains slightly higher at such site.

Some previous works have reported the peak dose rate and the accumulated dose for the (different, or multiple) events of the Halloween storm at different locations (Jiggens et al., 2014; Joyce et al., 2015; Kozarev et al., 2010; PourArsalan et al., 2010; Schwadron et al, 2010). Importantly, *near Earth*, for the spectra of a 1-in-20-year event from SEPEM (Jiggens et al., 2012) closely agreeing with that of the October 28, 2003 event, the accumulated dose was reported to be ∼0.2 Gy-Eq (133mGy) (Jiggens et al., 2014) behind 1 cm (linear thickness) Al-shielding, close to the BFO limit 0.25 Gy-Eq. As the weakest region of an Extra-Vehicular Activity (EVA) suit is 15 times lower than this Al equivalent, effective warning for astronauts on EVA at Earth would have been fundamental (Jiggens et al., 2014). Since the interplanetary space dose rates could be considered to represent the possible upper limit of the radiation exposure in which an astronaut is doing EVAs when a SEP event occurs (Guo, Zeitlin, et al., 2018), we can therefore easily conclude that the BFOs limit would have been overpassed at Mars for the October 28, 2003 event, similarly to conclusions from previous studies on the October 26, 2003 event (PourArsalan et al., 2010). While the atmosphere stops most of the SEPs, especially the low-energy ones, the latter do contribute greatly to the unshielded deep space dose.

5. Conclusions

We have presented a Monte Carlo particle transport study of the radiation environment and doses at Oxia Planum, the landing site for ExoMars 2022, and at two locations at Mawrth Vallis, previously under scrutiny as candidate landing sites respectively for the ExoMars 2022 and the current MSL mission, during solar minimum and close to solar maximum during the declining phase of solar cycle 23, using the ESA's official model dMEREM. The dMEREM standalone version available to users, via ESA's permission, was used and some post-processing tools were implemented to allow to use of different vertical profiles from MCD and to calculate the absorbed dose (not automatically printed by dMEREM). The results may serve as reference for future measurements from the Liulin-ML detector on the ExoMars 2022 surface platform and point to some differences with respect to the results from previous analysis of RAD data for Gale crater.

The radiation environments among the three sites appear, overall, similar. The comparison of the daily ADE and absorbed dose rates with the updated extrapolation from RAD data highlights the importance of some differences in the input modulation conditions, especially for solar minimum, considered in the present calculations and in the analysis of RAD data, intrinsic limitations of the ISO15390 model in describing accurately the flux of primary light ions, and the neglect of heavier ions in our work which may affect both the results for solar minimum and those for solar maximum. Small differences are found in the γ-rays contribution at Oxia Planum and Mawrth Vallis site 2. In particular, neutrons contribute more to the ADE rates at the deepest Mawrth Vallis site 2, due to increased fragmentation in the downward cascade. However, in the backscattered components, a ∼10% increase of water content at Mawrth Vallis 2 with respect to Oxia Planum moderates more efficiently fast neutrons. With more moderated neutrons, γ-rays in the backscattered component generated in neutron capture reactions are slightly enhanced. The higher water content

at Mawrth Vallis and the consequent increased neutron modulation overweighs the eventual decreasing of neutrons solely given by Fe-oxides, given the small difference in hematite content at the two sites. The fact that γ-radiation may increase in presence of a more hydrated soil should be considered when considering the capability of minerals/materials to shield from radiation at specific sites, in the study of the shielding of biological molecules from radiation by mineral matrices, and in the consideration of possible scenarios for ISRU activities at sites with a mineralogy dominated by hydrated minerals.

In studying the dependence of doses on surface pressure, we only obtain a partial agreement with previous extrapolations from RAD data for different solar modulation conditions. An anti-correlation between ADE and absorbed dose day/night daily rates and surface pressure is found for both solar minimum and maximum. For solar minimum, this is in line with (Guo, Zeitlin, et al., 2018). For solar maximum, we only observe a weakening of such anti-correlation, or actually nearly coinciding dose rates, for both sites, contrary to the correlation reported by previous works. A slightly higher day/night pressure variation and ADE day/night daily rate variation at Oxia Planum could be related to a higher difference in the density vertical profiles above Oxia Planum in the dusty northern winter close to solar maximum. The present results suggest that not all the trends in the variation of doses reported by RAD could be similarly reproduced for the nothern hemisphere in the different seasons, and for sites with different dust loading.

The comparison of the results for a long (1-year) and short (30-days) surface stay suggests reasonable agreement with previous results from dMEREM (McKenna-Lawlor, Gonçalves, Keating, Morgado, et al., 2012), and for solar maximum with HZETRN (L. Simonsen, 1997) and PLANETOCOSMICS (Gronoff et al., 2015). The atmosphere of Mars provides a sufficient amount of shielding from the October 28, 2003 event, and incurred doses are below permissible limits, despite the considerably higher fluence with respect to the relevant September 2017 event detected by RAD. However, in reality the Halloween event featured multiple interplanetary shocks and ICMEs (Kozarev et al., 2010), which should be taken into account for late stochastic effects, in addition to the contribution from background GCRs. The influence of dust loading induces a variation with respect to the baseline MY26 scenario similar to previous studies (Norman et al., 2014).

Further work is needed to better discern the causes of the differences with the data from RAD at Gale crater, in particular by adding heavier ions and also possibly disentangling seasonal effects, that is effects of the CO_2 condensation cycle. At the same time, additional work would be needed to investigate the impact of a higher simultaneous variation of water and Fe-content for sites at different elevation on the doses at the surface and, possibly, in the subsurface.

Data Availability Statement

The data relative to Figures 2–7 can be found at the Zenodo platform (Da Pieve et al., 2020, figure data for "Radiation environment and doses on Mars at Oxia Planum and Mawrth Vallis: support for exploration at sites with high biosignature preservation potential" Zenodo, 10.5281/zenodo.3779187). The GCR spectra in Figure 1 can be retrieved from the SPENVIS interface (https://www.spenvis.oma.be/) and the differential profile fluxes for the October–November 2003 period from the SEPEM tool (http://sepem.eu/).

Acknowledgments
The authors acknowledge Dr. Hugh Evans (European Space Research and Technology Centre, ESEA, the Netherlands) for providing a standalone version of dMEREM, Dr. Ian Thomas (Royal Belgian Institute of Space Aeronomy, Belgium) for help with the SPICE-enhanced version of the visualization tool Cosmographia (https://naif.jpl.nasa.gov/naif/cosmographia.html) and Dr. Vincent Letocart (Royal Belgian Institute for Space Aeronomy, Belgium) for assistance for computational aspects. J. G. is supported by the Strategic Priority Program of the Chinese Academy of Sciences (Grant No. XDB41000000 and XDA15017300), the National Natural Science Foundation of China (Grant No. 42074222) and the CNSA pre-research Project on Civil Aerospace Technologies (Grant No. D020104). The work has received fundings from the Research Executive Agency under the EU's Horizon 2020 Research and Innovation program (grant ID 776410). This work benefited from networking activities carried out within the EU funded COST Action CA17126 (TUMIEE) and represents a contribution to it. G. Gronoff and C. J. Mertens were supported by the Advanced Exploration Systems Division within the NASA Human Exploration and Operations Mission Directorate. We acknowledge the RAD data which are archived in the NASA planetary data systems' planetary plasma interactions node (http://ppi.pds.nasa.gov/).

References

Agostinelli, S., Allison, J., Amako, K., Apostolakis, J., Araujo, H., Arce, P., et al. (2003). Geant4—A simulation toolkit. *Nuclear Instruments Methods Physics Research Section A: Accelerators, Spectrometers, Detectors and Associated Equipment*, *506*(3), 250–303.

Allen, C. C., Westfall, F., & Schelble, R. T. (2004). Importance of a martian hematite site for astrobiology. *Astrobiology*, *1*(1). https://doi.org/10.1089/153110701750137495

Anno, G. H., Baum, S. J., Withers, H. R., Young, R. W., Young, R. W., & Young, R. W. (1989). Symptomatology of acute radiation effects in humans after exposure to doses of 0.5-30 Gy. *Health Physics*, *56*, 821–838.

Bridges, D., Loizeau, D., Sefton-Nash, E., Vago, J., Williams, R., Balme, M., et al. (2017). Selection and characterisation of the exomars 2020 rover landing sites. 48th Lunar Planet. Sci. Conf. 2378 (Lunar and Planetary Institute).

Carter, J., Poulet, F., Bibring, J.-P., Mangold, N., & Murchie, S. (2013). Hydrous minerals on Mars as seen by the CRISM and OMEGA imaging spectrometers: Updated global view. *Journal of Geophysical Research: Planets*, *118*(4), 831–858. https://doi.org/10.1029/2012je004145

Casimiro, A. L., Sampaio, J. M., & Gonçalves, P. (2018). Assessment of radiation exposure in manned missions to Mars for three profiles. *Radiation & Applications*, *3*, 27–33.

Chenglong, S., Yuming, W., Pinzhong, Y., & Wang, S. (2008). Enhancement of solar energetic particles during a shock-magnetic cloud interacting complex structure. *Solar Physics*, *252*, 409–418.

Cohen, C. M. S., & Mewaldt, R. A. (2018). The ground-level enhancement event of September 2017 and other large solar energetic particle events of cycle 24. *Space Weather*, *16*(10), 1616–1623.
Crider, D. H., Espley, J., Brain, D. A., Mitchell, D. L., Connerney, J. E. P., & Acuña, M. H. (2005). Mars Global Surveyor observations of the Halloween 2003 solar superstorm's encounter with Mars. *Journal of Geophysical Research: Space Physics*, *110*(A9). https://doi.org/10.1029/2004ja010881
Cucinotta, F. A., Alp, M., Rowedder, B., & Kim, M.-H. Y. (2015). Safe days in space with acceptable uncertainty from space radiation exposure. *Life Sciences and Space Research*, *5*, 31–38.
Cucinotta, F. A., et al. (2001). Space radiation cancer risks and uncertainties for Mars missions. *Radiation Research*, *156*, 682–688.
Cucinotta, F. A., Kim, M.-H. Y., & Ren, L. (2006). Evaluating shielding effectiveness for reducing space radiation cancer risks. *Radiation Measurements*, *41*(9-10), 1173–1185. https://doi.org/10.1016/j.radmeas.2006.03.011
Cucinotta, F. A., Kim, M. Y., & Chappell, L. J. (2012b). Space radiation cancer risk projections and uncertainties. NASA/TP-2013-217375, 5, 2013-21737.
Dartnell, L. R., Desorgher, L., Ward, J. M., & Coates, A. J. (2007). Modelling the surface and subsurface Martian radiation environment: Implications for astrobiology. *Geophysical Research Letters*, *34*(2). https://doi.org/10.1029/2006gl027494
De Angelis, G., Wilson, J., Clowdsley, M., Qualls, G., & Singleterry, R. (2006). Modeling of the Martian environment for radiation analysis. *Radiation Measurements*, *41*(9), 1097–1102.
de Wet, W., & Townsend, L. (2017). A calculation of the radiation environment on the Martian surface. *Life Sciences and Space Research*, *14*, 51–56.
Desorgher, L. (2005). *Planetocosmics software user manual*. (Accessible from the GEANT4/PLANETOCOSMICS web page).
dos Santos, R., Patel, M., Cuadros, J., & Martins, Z. (2016). Influence of mineralogy on the preservation of amino acids under simulated Mars conditions. *Icarus*, *277*, 342–353.
Ehresmann, B., Burmeister, S., Wimmer-Schweingruber, R. F., & Reitz, G. (2011). Influence of higher atmospheric pressure on the Martian radiation environment: Implications for possible habitability in the Noachian epoch. *Journal of Geophysical Research: Space Physics*, *116*(A10). https://doi.org/10.1029/2011ja016616
Ertem, G., Ertem, M., McKay, C., & Hazen, R. (2017). Shielding biomolecules from effects of radiation by Mars analogue minerals and soils. *International Journal of Astrobiology*, *16*, 280–285.
Feynman, J., Ruzmaikin, A., & Berdichevsky, V. (2002). The JPL proton fluence model: An update. *Journal of Atmospheric and Terrestrial Physics*, *64*, 1679–1686.
Feynman, J., Spitale, G., Wang, J., & Gabriel, S. (1993). Interplanetary proton fluence model: JPL 1991. *Journal of Geophysical Research: Space Physics*, *98*(A8), 13281–13294. https://doi.org/10.1029/92ja02670
Flores-McLaughlin, J. (2017). Radiation transport simulation of the Martian GCR surface flux and dose estimation using spherical geometry in PHITS compared to MSL-RAD. *Life Sciences and Space Research*, *14*, 36–42.
Fontenot, J., Taddei, P., Zheng, Y., Mirkovic, D., & Newhauser, W. D. (2009). Ambient dose equivalent versus effective dose for quantifying stray radiation exposures to a patient receiving proton therapy for prostate cancer. *Nuclear Technology*, *168*(1), 173–177.
Forget, F., Hourdin, F., Fournier, R., Hourdin, C., Talagrand, O., Collins, M., et al. (1999). Improved general circulation models of the Martian atmosphere from the surface to above 80 km. *Journal of Geophysical Research: Planets*, *104*(E10), 24155–24175. https://doi.org/10.1029/1999je001025
Forget, F., Millour, E., Lebonnois, S., Montabone, L., Dassas, K., Lewis, S., et al. (2006). *The new Mars Climate Database 2nd workshop on Mars atmosphere, modeling, and observations*. Spain: Granada.
Gonçalves, P., Keating, A., Valente, S., Truscott, P., Lei, F., Desorgher, L., et al. (2010). Mars rem: The mars energetic radiation environment models. In P. Lodz (Ed.), *Proceedings of the 31st international cosmic ray conference*.
Gronoff, G., Norman, R. B., & Mertens, C. (2015). Computation of cosmic ray ionization and dose at Mars. I: A comparison of HZETRN and Planetocosmics for proton and *a* particles. *Advances in Space Research*, *55*(7), 1799–1805.
Gross, C., Carter, J., Poulet, F., Loizeau, D., Bishop, J., Horgan, B., et al. (2017). Mawrth vallis: An auspicious destination for the esa and nasa 2020 landers. In 48th Lunar Planet Sci. Conf. 2378 (Lunar and Planetary Institute).
Grotzinger, J. P., Crisp, J., Vasavada, A. R., Anderson, R. C., Baker, C. J., et al. (2012). Mars Science Laboratory mission and science investigation. *Space Science Reviews*, *170*(1–4), 5–56.
Guidance on Radiation Received in Space Activities. Bethesda, Md. (Tech. Rep.) (1989). National Council on radiation protection and measurements Rep. 98.
Guo, J., Dumbović, M., Wimmer-Schweingruber, R. F., Temmer, M., Lohf, H., Wang, Y., et al. (2018a). Modeling the Evolution and Propagation of 10 September 2017 CMEs and SEPs Arriving at Mars Constrained by Remote Sensing and In Situ Measurement. *Space Weather*, *16*(8), 1156–1169. https://doi.org/10.1029/2018sw001973
Guo, J., Saša, B., Röstel, L., Terasa, J. C., Herbst, K., Heber, B., et al. (2019a). Implementation and validation of the GEANT4/AtRIS code to model the radiation environment at Mars. *Space Weather Space Clim*, *9*, A2. https://doi.org/10.1051/swsc/2018051
Guo, J., Slaba, T. C., Zeitlin, C., Wimmer-Schweingruber, R. F., Badavi, F. F., Böhm, E., et al. (2017). Dependence of the Martian radiation environment on atmospheric depth: Modeling and measurement. *Journal of Geophysical Research: Planets*, *122*(2), 329–341. https://doi.org/10.1002/2016je005206
Guo, J., Wimmer-Schweingruber, R., Wang, Y., Grande, M., Matthiä, D., Zeitlin, C., et al. (2019b). The pivot energy of Solar Energetic Particles Affecting the Martian surface radiation environment. *The Astrophysical Journal*, *883*(L12).
Guo, J., Zeitlin, C., Wimmer-Schweingruber, R. F., McDole, T., Kiihl, P., Appel, J. C., et al. (2018b). Generalized approach to model the spectra and radiation dose rate of solar particle events on the surface of Mars. *The Astronomical Journal*, *155*(49), 15.
Guo, J., Zeitlin, C., Wimmer-Schweingruber, R. F., Rafkin, S., Hassler, D. M., Posner, A., et al. (2015). Modeling the variations of Dose Rate measured by RAD during the first MSL Martian year: 2012–2014. *The Astrophysical Journal*, *810*(1), 24.
Haberle, R., Gomez-Elvira, J., Juarez, M. T., Harri, A.-M., Hollingsworth, J., Kahanpää, H., et al. (2014). Preliminary interpretation of the REMS pressure data from the first 100 sols of the MSL mission. *Journal of Geophysical Research: Planets*, *119*(3), 440–453.
Hassler, D. M., Zeitlin, C., Ehresmann, B., Wimmer-Schweingruber, R. F., Guo, J., Matthiä, D., et al. (2018). Space weather on the surface of Mars: Impact of the September 2017 events. *Space Weather*, *16*.
Hassler, D., Zeitlin, C., Wimmer-Schweingruber, R., Bottcher, S., Martin, C., et al. (2012). The Radiation Assessment Detector (RAD) investigation. *Space Science Reviews*, *170*(1–4), 503–558.
Hassler, D. M., Zeitlin, C., Wimmer-Schweingruber, R. F., Ehresmann, B., Rafkin, S., Eigenbrode, J. L., et al. (2014). Mars' surface radiation environment measured with the Mars Science Laboratory's curiosity rover. *Scientific Reports*, *343*, 1244797.

Heynderickx, D., Quaghebeur, B., Wera, J., Daly, E., & Evans, H. (2004). New radiation environment and effect models in ESA's space environment information system (SPENVIS). *Space Weather*, *2*, S10s03.
ICRP. (2010). Conversion coeffients for radiological protection quantities for external radiation exposures. icrp publication 116. *Annals of the ICRP*, *40*(2–5), 1–257.
Jiggens, P., Chavy-Macdonald, M.-A., Santin, G., Menicucci, A., Evans, H., & Hilgers, A. (2014). The magnitude and effects of extreme solar particle events. *The Journal of Space Weather and Space Climate*, *4*, A20.
Jiggens, P., Gabriel, S., Heynderickx, D., Crosby, N., Glover, A., & Hilgers, A. (2012). ESA SEPEM project: Peak flux and fluence model. *IEEE Transactions on Nuclear Science*, *59*, 1066–1077.
Joyce, C. J., Schwadron, N. A., Townsend, L. W., Mewaldt, R. A., Cohen, C. M. S., von Rosenvinge, T. T., et al. (2015). Analysis of the potential radiation hazard of the 23 July 2012 SEP event observed by STEREO A using the EMMREM model and LRO/CRaTER. *Space Weather*, *13*(9), 560–567. https://doi.org/10.1002/2015sw001208
Keating, A., & Gonçalves, P. (2012). The impact of Mars geological evolution in high energy ionizing radiation environment through time. *Planetary and Space Science*, *72*(1), 70–77.
Keil, R., & Mayer, L. (2014). 12.12 - mineral matrices and organic matter. In H. D. Holland, & K. K. Turekian (Eds.), *Treatise on geochemistry*. 2nd ed. (pp. 337–359). Oxford: Elsevier.
Kozarev, K., Schwadron, N. A., Dayeh, M. A., Townsend, L. W., Desai, M. I., & PourArsalan, M. (2010). Modeling the 2003 Halloween events with EMMREM: Energetic particles, radial gradients, and coupling to MHD. *Space Weather*, *8*, S00E08. https://doi.org/10.1029/2009SW000550$
Kruglanski, M., Messios, N., De Donder, E., Gamby, E., Calders, S., Hetey, L., et al. (2009). Last upgrades and development of the space environment information system (SPENVIS). Proceedings of the European Conference on radiation and its effects on components and systems, RADECS, 563-565. https://doi.org/10.1109/RADECS.2009.5994715
Lario, D., Decker, R. B., Livi, S., Krimigis, S. M., Roelof, E. C., Russell, C. T., & Fry, C. D. (2005). Heliospheric energetic particle observations during the October-November 2003 events. *Journal of Geophysical Research: Space Physics*, *110*(A9), https://doi.org/10.1029/2004ja010940
Lee, C., Lawson, W., Richardson, M., Heavens, N., Kleinboh, A., Banfield, D., et al. (2009). Thermal tides in the Martian middle atmosphere as seen by the Mars climate sounder. *Journal of Geophysical Research*, *114*, E03005. https://doi.org/10.1029/2008JE003285
Leovy, C. B., & Zurek, R. W. (1979). Thermal tides and Martian dust storms: Direct evidence for coupling. *Journal of Geophysical Research*, *84*(B6), 2956. https://doi.org/10.1029/jb084ib06p02956
Martínez, G., Newman, C., De Vicente-Retortillo, A., Fischer, E., Renno, N., Richardson, M., et al. (2017). The modern near-surface Martian climate: A review of in-situ meteorological data from Viking to Curiosity. *Space Science Reviews*, *212*, 295–338.
Masarik, J., & Reedy, R. (1996). Gamma ray production and transport in Mars. *Journal of Geophysical Research*, *101*, 18891–18912. https://doi.org/10.1029/96JE01563
Matthiä, D., & Berger, T. (2017). The radiation environment on the surface of Mars - Numerical calculations of the galactic component with GEANT4/PLANETOCOSMICS. *Life Sciences and Space Research 14*, 57–63.
Matthiä, D., Ehresmann, B., Lohf, H., Kohler, J., Zeitlin, C., Appel, J, et al. (2016). The Martian surface radiation environment - a comparison of models and MSL/RAD measurements. *The Journal of Space Weather and Space Climate.6*, A13
Matthiä, D., Hassler, D., de Wet, W., Ehresmann, B., Firan, A., Flores-McLaughlin, J., et al. (2017). The radiation environment on the surface of Mars–Summary of model calculations and comparison to RAD data. *Life Sciences and Space Research*, *14*, 18–28.
McKenna-Lawlor, S., Gonçalves, P., Keating, A., Morgado, B., Heynderickx, D., Nieminen, P., et al. (2012). Characterization of the particle radiation environment at three potential landing sites on Mars using ESAs MEREM models. *Icarus*, *218*(1), 723–734.
McKenna-Lawlor, S., Gonçalves, P., Keating, A., Reitz, G., & Matthiä, D. (2012). Overview of energetic particle hazards during prospective manned missions to Mars. *Planetary and Space Science*, *63–64*, 123–132.
Medvedev, A. S., Kuroda, T., & Hartogh, P. (2011). Influence of dust on the dynamics of the Martian atmosphere above the first scale height. *Aeolian Research*, *3*(2), 145–156.
Mertens, C. J. (2016). Overview of the radiation dosimetry experiment (RaD-X) flight mission. *Space Weather*, *14*(11), 921–934.
Mertens, C. J., Gronoff, G. P., Norman, R. B., Hayes, B. M., Lusby, T. C., Straume, T., et al. (2016). Cosmic radiation dose measurements from the RaD-X flight campaign. *Space Weather*, *14*(10), 874–898. https://doi.org/10.1002/2016sw001407
Mewaldt, R. A., Cohen, C. M. S., Labrador, A. W., Leske, R. A., Mason, G. M., Desai, M. I., et al. (2005). Proton, helium, and electron spectra during the large solar particle events of October-November 2003. *Journal of Geophysical Research: Space Physics*, *110*, A09S18. https://doi.org/10.1029/2005ja011038
Mrigakshi, A. I., Matthiä, D., Berger, T., Reitz, G., & Wimmer-Schweingruber, R. F. (2013). How Galactic Cosmic Ray models affect the estimation of radiation exposure in space. *Advances in Space Research*, *51*(5), 825–834. https://doi.org/10.1016/j.asr.2012.10.017
Mrigakshi, A. I., Matthiä, D., Berger, T., Reitz, G., & Wimmer-Schweingruber, R. F. (2012). Assessment of galactic cosmic ray models. *Journal of Geophysical Research: Space Physics*, *117*(A8). https://doi.org/10.1029/2012ja017611
National Council on Radiation Protection and Measurements, Recommendations of Dose Limits for Leo (Tech. Rep.) (2000). NCRP Rep. 132.
Neary, L., & Daerden, F. (2018). The GEM-Mars general circulation model for Mars: Description and evaluation. *Icarus*, *300*, 458–476.
Nockolds, S. (1954). Average chemical compositions of some igneous rocks. *The Geological Society of America Bulletin*, *65*, 1007.
Norman, R. B., Gronoff, G., & Mertens, C. (2014). Influence of dust loading on atmospheric ionizing radiation on Mars. *Journal of Geophysical Research A: Space Physics*, *119*(1), 452–461. https://doi.org/10.1002/2013JA019351
Norman, R. B., Mertens, C. J., & Slaba, T. C. (2016). Evaluating galactic cosmic ray environment models using RaD-X flight data. *Space Weather*, *14*(10), 764–775.
Nymmik, R. A., Panasyuk, M. I., & Suslov, A. A. (1996). Galactic cosmic ray flux simulation and prediction. *Advances in Space Research*, *17*, 19–30.
Operational Radiation Safety Program for Astronauts in Low-Earth Orbit: A Basic Framework. Bethesda, Md. (Tech. Rep.). (2002). National Council on radiation protection and measurements Rep. 142.
Osamu, S., Yosiiizawa, N., Takagi, S., Iwai, S., Ueittara, T., Sakamoto, Y., et al. (1999). Calculations of effective dose and ambient dose equivalent conversion coefficients for high energy photons. *Journal of Nuclear Science and Technology*, *36*(11), 977–987.
Pavlov, A. K., Blinov, A. V., & Konstantinov, A. N. (2002). Sterilization of Martian surface by cosmic radiation. *Planetary and Space Science*, *50*(7-8), 669–673. https://doi.org/10.1016/s0032-0633(01)00113-1
Pavlov, A. K., Vasilyev, G., Ostryakov, V. M., Pavlov, A. K., & Mahaffy, P. (2012). Degradation of the organic molecules in the shallow subsurface of Mars due to irradiation by cosmic rays. *Geophysical Research Letters*, *39*(L13202).

Pelliccioni, M. (2000). Overview of fluence-to-effective dose and fluence-to-ambient dose equivalent conversion coefficients for high energy radiation calculated using the FLUKA code. *Radiation Protection Dosimetry*, *88*(4), 279–297.

Poulet, F., Gross, C., Horgan, B., Loizeau, D., Bishop, J. L., Carter, J., et al. (2020). Mawrth Vallis, Mars: A fascinating place for future in situ exploration. *Astrobiology*, *20*(2), 199–234. https://doi.org/10.1089/ast.2019.2074

PourArsalan, M., Townsend, L. W., Schwadron, N. A., Kozarev, K., Dayeh, M. A., & Desai, M. I. (2010). Time-dependent estimates of organ dose and dose equivalent rates for human crews in deep space from the 26 October 2003 solar energetic particle event (Halloween event) using the Earth-Moon-Mars Radiation Environment Module. *Space Weather*, *8*, S00E05.

Rafkin, S. C. R., Zeitlin, C., Ehresmann, B., Hassler, D., Guo, J., Köhler, J., et al. (2014). Diurnal variations of energetic particle radiation at the surface of Mars as observed by the Mars Science Laboratory Radiation Assessment Detector. *Journal of Geophysical Research: Planets*, *119*(6), 1345–1358. https://doi.org/10.1002/2013je004525

Ratliff, H. N., Smith, M. B. R., & Heilbronn, L. H. (2017). Simulation of the GCR spectrum in the Mars curiosity rover's RAD detector using MCNP6. *Life Sciences and Space Research*, *14*.

Richardson, M. I., & Newman, C. E. (2018). On the relationship between surface pressure, terrain elevation, and air temperature. Part I: The large diurnal surface pressure range at Gale Crater, Mars and its origin due to lateral hydrostatic adjustment. *Planetary and Space Science*, *164*(1), 132–157.

Rogers, A. D., & Bandfield, J. L. (2009). Mineralogical characterization of Mars Science Laboratory candidate landing sites from THEMIS and TES data. *Icarus*, *203*(2), 437–453.

Röstel, L., Guo, J., Banjac, S., Wimmer-Schweingruber, R. F., & Heber, B. (2020). Subsurface radiation environment of Mars and its implication for shielding protection of future habitats. *Journal of Geophysics: Planets*, *125*, e2019JE006246. https://doi.org/10.1029/2019JE006246

Saganti, P. B., Cucinotta, F. A., Wilson, J. W., Simonsen, L. C., & Zeitlin, C. (2004). Radiation climate map for analyzing risks to astronauts on the Mars surface from galactic cosmic rays. *Space Science Reviews*, *110*(1–2), 143–156.

Schwadron, N. A., Boyd, A. J., Kozarev, K., Golightly, M., Spence, H., Townsend, L. W., & Owens, M. (2010). Galactic cosmic ray radiation hazard in the unusual extended solar minimum between solar cycles 23 and 24. *Space Weather*, *8*, S00E04. https://doi.org/10.1029/2010SW000567

Semkova, J., Koleva, R., Benghin, V., Dachev, T., Matviichuk, Y., Tomov, B., et al. (2018). Charged particles radiation measurements with Liulin-MO dosimeter of FREND instrument aboard ExoMars Trace Gas Orbiter during the transit and in high elliptic Mars orbit. *Icarus*, *303*, 53–66.

Simonsen, L. (1997). Analysis of lunar and mars habitation modules for the space exploration initiative. Shielding strategies for human space exploration (Vol. *4*). NASA CP-3360.

Simonsen, L. C., & Nealy, J. (1993). Mars surface radiation exposure for solar maximum conditions and 1989 solar proton events. NASA Technical Paper Series, 3300.

Simonsen, L., Nealy, J., & Townsend, L. J. (1990). Radiation exposure for manned Mars surface missions. NASA Technical Paper Series, NASA-TP- 2979, L-16708, 24, Document 1.

Simpson, J. A. (1983). Elemental and isotopic composition of the galactic cosmic rays. *Annual Review of Nuclear and Particle Science*, *33*, 323–382.

Slaba, T. C., & Stoffle, N. N. (2017). Evaluation of HZETRN on the Martian surface: Sensitivity tests and model results. *Life Sciences and Space Research*, *14*.

Smith, D. E., Zuber, M. T., Frey, H. V., Garvin, J. B., Head, J. W., Muhleman, D. O., et al. (2001). Mars orbiter laser altimeter: Experiment summary after the first year of global mapping of Mars. *Journal of Geophysical Research*, *106*(E10), 23689–23722. https://doi.org/10.1029/2000JE001364

Townsend, L., PourArsalan, M., Hall, M., Anderson, J., Bhatt, S., DeLauder, N., et al. (2011). Estimates of Carrington-class solar particle event radiation exposures on Mars. *Acta Astronautica*, *69*(7), 397–405.

Wu, H., Huff, J., Casey, R., Kim, M.-H., & Cucinotta, F. (2009). *Risk of acute radiation syndromes due to solar particle events*. Houston: NASA Johnson Space Center. hrp-47052.

Zeitlin, C., Boynton, W., Mitrofanov, I., Hassler, D., Atwell, W., Cleghorn, T. F., et al. (2010). Mars Odyssey measurements of galactic cosmic rays and solar particles in Mars orbit, 2002–2008. *Space Weather*, *8*(11). https://doi.org/10.1029/2009SW000563

Zeitlin, C., Hassler, D. M., Guo, J., Ehresmann, B., Wimmer-Schweingruber, F. R., Rafkin, S. C. R., et al. (2018). Analysis of the radiation hazard observed by RAD on the surface of Mars during the September 2017 solar particle event. *Geophysical Research Letters*, *45*, 5845–5851. https://doi.org/10.1029/2018GL077760